Nonlinear restoring force of spring with stopper for ferroelectric dipole electret-based electrostatic vibration energy harvesters

Nonlinear restoring force of spring with stopper for ferroelectric dipole electret-based electrostatic vibration energy harvesters

H. Asanuma,[1,a] M. Hara,[2] H. Oguchi,[2,3,4] and H. Kuwano[2]
[1]*Faculty of Mechanical Engineering, Institute of Science and Engineering, Kanazawa University, Kakuma-machi, Kanazawa 920-1192, Japan*
[2]*Department of Nanomechanics, Tohoku University, 6-6-01, Aoba, Aramaki, Aza-Aoba, Sendai 980-8579, Japan*
[3]*Micro System Integration Center (μSIC), Tohoku University, 6-6-01, Aoba, Aramaki, Aza-Aoba, Sendai 980-8579, Japan*
[4]*Advanced Institute for Materials Research (AIMR), Tohoku University, 2-2-1, Aoba, katahira, Sendai 980-8577, Japan*

(Received 11 May 2016; accepted 4 July 2016; published online 11 July 2016)

Previously, we succeeded in developing a new electret [termed a ferroelectric dipole electret (FDE)] having an extremely high electric field using a polarized ferroelectric material. However, the pull-in, in which an oscillator sticks to the FDE under its strong electrostatic force, poses a problem for practical vibration energy harvesters. In this study, we propose use of nonlinear restoring force of a spring with a stopper in order to prevent pull-in for FDE-based vibration energy harvesters. The spring with a stopper was designed using a finite element method (FEM) analysis such that the restoring force of the spring will exceed the electrostatic force of the FDE. The proposed harvester combines the FDE and the spring successfully, and generated electricity without the pull-in. It also showed the highest figure of merit of output power and wide frequency band when compared with other available electret-based vibration energy harvesters. [http://dx.doi.org/10.1063/1.4958884]

I. INTRODUCTION

Recently, the Internet of Things or the Trillion Sensor Universe has drawn considerable attention.[1] This system is built by extensively deploying and wirelessly connecting sensor modules, each of which mainly consists of a micro sensor, an electronic controller, a wireless transmission device, and a power source. One immediate demand for realization of the system is the development of miniaturized power sources that do not require maintenance or electrical wiring. Electrostatic vibration energy harvesters (VEHs) using charged dielectrics, referred to as "electrets", represent one promising power source given that they are suited to miniaturization because of their compatibility with MEMS processing. However, their lower output power[2] compared with that for other transductions (piezoelectric,[3] electromagnetic,[4] or inverse magnetostrictive[5]) is a key issue.

To enhance the output power for electret-based VEHs, we have recently put forth a new electret from a polarized ferroelectric material [hereafter, termed a ferroelectric dipole electret (FDE)] that can generate much higher electric fields than conventional polymer-based or inorganic silicon-based electrets. Thanks to the high electric field, the harvester employing the FDE exhibits a three-fold increase in output power density over that of a CYTOP polymer-based electret.[6] In our previous studies, the output power was evaluated using a simple experimental set-up, briefly described as follows. The FDE is affixed to the lower electrode, which is attached to a shaker that controls

[a]Author to whom correspondence should be addressed. Electronic mail: h-asanuma@se.kanazawa-u.ac.jp

out-of-plane vibration. The second, stationary, upper electrode is placed separately from the shaker, facing the FDE across the air gap.[6–8] The initial air gap (center of the out-of-plane vibration) between the upper electrode and the FDE was set to 0.35 mm, and the applied frequency, acceleration, and peak-to-peak amplitude of the out-of-plane vibration were set to 20 Hz, 4.9 m/s^2, and 0.62 mm, respectively. Because the upper electrode is held fixed in this simple harvester structure, during the evaluation there is no need to consider pull-in,[9] in which the upper electrode sticks to the FDE under its attractive electrostatic forces. For this reason, the minimum air gap of 0.04 mm and thus high normalized output power of 78 μW/cm^3 were achieved. However, pull-in poses a serious problem in practical harvester designs in which an upper electrode oscillates from external vibration, because the restoring force of a linear spring linked with the upper electrode cannot resist the FDE's attractive electrostatic forces, which will rapidly increase as the upper electrode moves closer to the FDE. To realize the full potential of the FDE advantages, a spring that can avoid pull-in needs to be developed. In this study, we first design a spring that can resist the strong attractive electrostatic force of the FDE and then demonstrate a high-performance VEH by combining the FDE and the designed spring.

II. DESIGN AND FABRICATION

First, we evaluate the strength of the FDE electrostatic force. In this study, we roughly estimate the strength of the FDE electrostatic force by static analysis. Figure 1 shows schematic model and its equivalent circuit of the FDE-based harvester in static states. The FDE was attached on the lower electrode, and set to face up negatively charged top surface against an upper electrode. Unlike polymer-based or inorganic silicon-based electrets charged by implanting single excess charges,[2,10] FDEs are charged through dipole orientation, in which the FDEs inherently have positive and negative charges on the opposite surfaces.[6] Thus, as shown in Figure 1(b), the dipole characteristics of the FDE forms an ultrathin capacitor C' between the lower electrode and the positively charged bottom surface of the FDE. Based on Kirchhoff's voltage law and the parallel plate capacitor model, the electrostatic force F_{ele} of the FDE in static states can be calculated from the following equation:

$$\left(\frac{1}{C'} + \frac{1}{C_{ele}} + \frac{1}{C_{air}(x)}\right) Q + V_s = \frac{Q}{C_{tot}} + V_s = 0, \tag{1}$$

$$F_{ele} = \frac{Q^2}{2\varepsilon_0 S} = \frac{{C_{tot}}^2 {V_s}^2}{2\varepsilon_0 S}, \tag{2}$$

where C_{ele} is the capacitance of the FDE, C_{air} is the air capacitance, C_{tot} is the series capacitance formed between the upper electrode and the lower electrode, x is the distance between the upper electrode and the top surface of the FDE, V_s is the surface potential of the FDE, Q is the induced charge on the upper electrode, ε_0 is the permittivity of air, and S is the area of the electrodes and of the FDE, respectively. C_{ele} is calculated from $\varepsilon_r\varepsilon_0 S/d$ (ε_r = 1460, S = 1 cm^2, and d = 1 mm), and

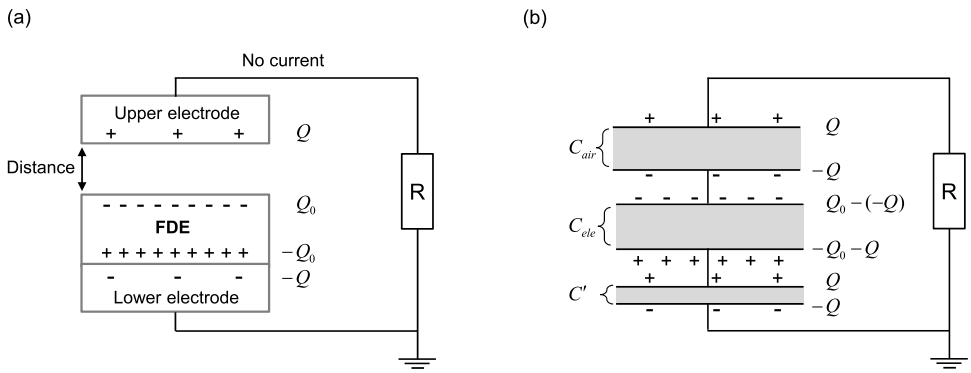

FIG. 1. (a) Schematic model and (b) its equivalent circuit of the FDE-based harvester in static states.

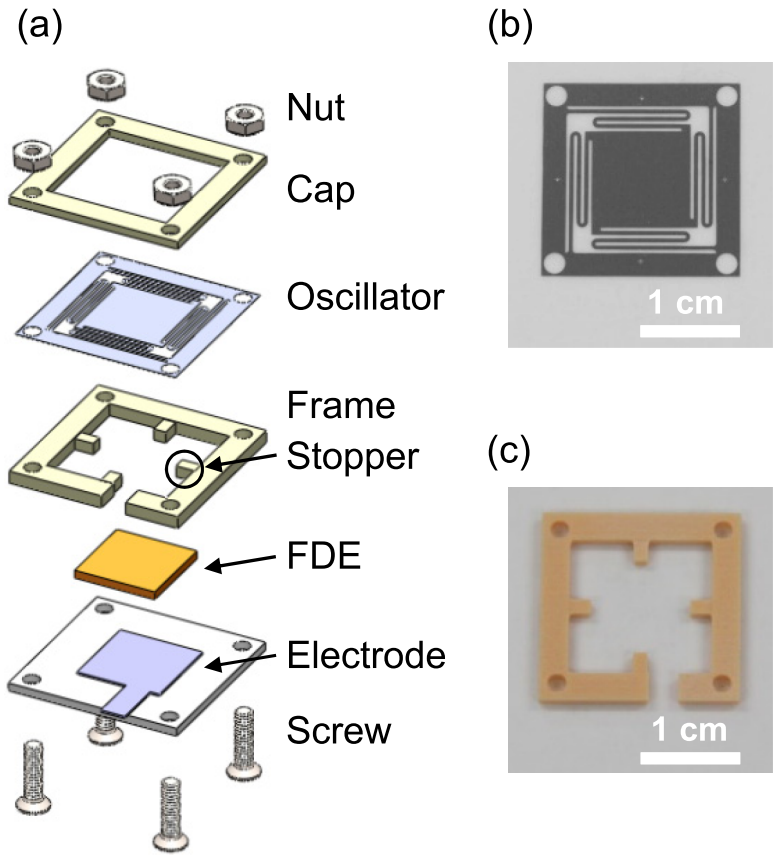

FIG. 2. (a) Schematic of the harvester assembly, (b) photograph of the oscillator, and (c) photograph of the frame.

V_s is -922 V. Thanks to its thickness, the value of C' is assumed to be much larger compared with C_{ele} and C_{air}. Therefore, in this study, we will calculate F_{ele}, ignoring the term of $1/C'$ in equation (1). This study will examine F_{ele} at x less than 100 μm, since the upper electrode needs to be located within a region that exhibits sufficiently large capacitance change and thus high output power. From this calculation, F_{ele} showed greater than tens of millinewtons per square centimeter at x less than 100 μm. Therefore, a spring should be designed such that its restoring force will exceed the tens of millinewtons per square centimeter within the distance.

To meet the requirements discussed above, we propose use of nonlinear restoring force of a spring with a stopper.[11–13] Figure 2 displays a schematic of the proposed harvester assembly and photographs of the oscillator and of the frame. As shown in Figure 2(a) and 2(c), the frame has four stoppers to contact the oscillator beams. After the beams contact the stoppers, the spring restoring force will increase rapidly because the effective length of the beam diminishes and thus the spring constant rapidly increases. The upper surface of the stopper and the lower surface of the oscillator are set at 170 μm and 270 μm above the FDE, respectively. The width of the stopper parallel to the beam length is 1.5 mm. The frame and the cap are formed by machine cutting from ABS resin. The oscillator is fabricated from a fine-grained stainless steel through photolithography.[10,14] The width, length, and thickness of the beam are 0.4, 30.8, and 0.08 mm, respectively. The area of the center square mass that also serves as the upper electrode is 1×1 cm^2, and the overall size of the harvester is $2 \times 2 \times 0.2$ cm^3.

Figure 3 shows an FEM analysis on the spring restoring force F_{spr} of the oscillator versus the distance between the position of the center square mass and the FDE. In this FEM analysis, we used COMSOL Multiphysics and its optional MEMS Module to consider the contact between the beam and the stopper. In the FEM analysis, the stopper is set as a rigid body and the beams of the oscillator is set as being elastic. The FEM analysis in Figure 3(b) shows that the effective contact

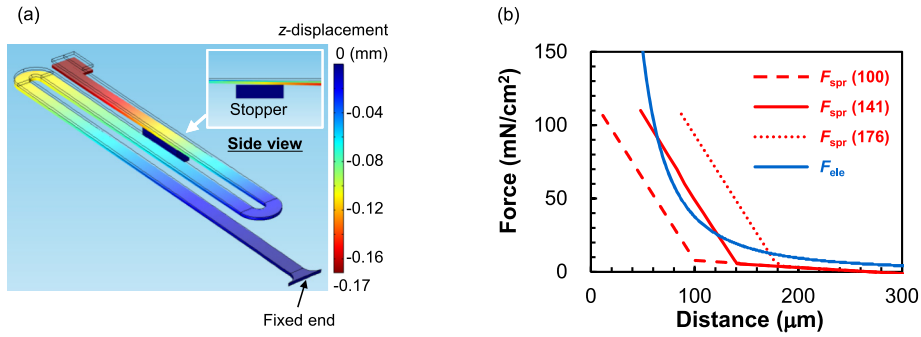

FIG. 3. FEM analysis: (a) typical results when the beam is in contact with the stopper and (b) spring restoring force F_{spr} of the oscillator at three different contact positions (100, 141, 176 μm) and the estimated electrostatic force F_{ele} of the FDE versus the distance between the position of the center square mass and the FDE.

position is 141 μm above the FDE, whereas the upper surface of the stopper is set at 170 μm above the FDE. The reason for this apparent discrepancy is that, as shown in the inset on Figure 3(a), the initial beam contact is not with the upper surface, but closer to the edge, of the stopper. The spring constant rapidly increases from 46 to 1120 N/m after contact, leading to the nonlinear enhancement of the spring restoring force. For comparison, we also plot the F_{ele} of the FDE estimated above and F_{spr} at different contact positions (100 μm and 176 μm) shown as a broken and a dotted line in Figure 3(b). For the contact position of 100 μm, F_{ele} that is stronger than F_{spr} will cause pull-in at a distance less than 100 μm. For the contact position of 176 μm, more than enough F_{spr} will stop the oscillator before it is located at a distance less than 100 μm, leading to low capacitance change and thus low output power. The restoring force of the designed spring for the contact position of 141 μm successfully exceeds the estimated electrostatic force of the FDE at distances from 60 to 100 μm. Therefore, the designed spring can prevent pull-in and achieve high output power for the FDE-based vibration energy harvester. As shown in Figure 3(b), in this design, the oscillator will rest at a distance of 124 μm, where F_{spr} of the oscillator and F_{ele} of the FDE are balanced. The oscillator can move when applied vibrational force is large enough to pull it away.

III. EXPERIMENTAL RESULTS AND DISCUSSION

Now we evaluate the output power, resonance frequency, and frequency bandwidth of the FDE-based vibration energy harvester under varying applied acceleration. The resistive load R is 50.5 MΩ, which is the impedance-matched value obtained in experiment. The output power P_{out} is evaluated from a time average:

$$P_{out} = \frac{1}{T}\int_0^T \frac{V_{out}{}^2}{R} dt, \tag{3}$$

where T is the measuring time period, and V_{out} is the output voltage across the resistive load.

The FDE was formed by poling a PZT ceramic (Fuji Ceramics Corp., Japan, No.C-2) at the poling electric field of 4 kV/mm. Detailed methodology for forming the FDE is reported in our previous studies.[6,8] The size of the FDE is $1 \times 1 \times 0.1$ cm^3. We use non-contacting electrostatic voltmeter (Trek Inc., Model 347) to measure the surface potential of FDEs. All measurements were performed after 24 hours following the poling treatment. The resulting surface potential V_s showed −922 V.

Figure 4 displays waveforms of oscillator displacement and output voltage at the resonance frequency of 139 Hz and the applied acceleration of 9.8 m/s^2. During vibration, we used a laser Doppler vibrometer (Ono Sokki, LV-1710 and LV-0712) to measure the oscillator displacement. In this measurement, the polarity of the displacement becomes positive when the oscillator moves downward to the FDE, and the polarity of the output voltage becomes positive when the current flows from the oscillator to the earth across the load. Because the designed nonlinear spring

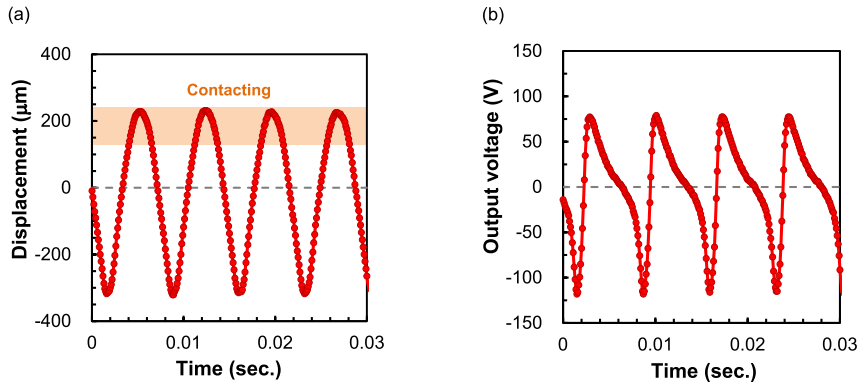

FIG. 4. Waveforms of (a) oscillator displacement and (b) output voltage at a resonance frequency f_r of 139 Hz and acceleration a of 9.8 m/s^2.

restoring force exceeds the FDE electrostatic force, our practical harvester successfully generated electricity without pull-in. As shown in Figure 4(a), an asymmetric waveform with respect to the zero-displacement dashed line is observed. This is attributed to the decreased displacement of the oscillator after contact with the stopper.

Figure 5 shows the output power P_{out} and peak-to-peak displacement $Disp_{p-p}$ of the oscillator versus frequency with varying acceleration a (2.0, 4.9, 6.9, and 9.8 m/s^2). The frequency was swept forward and downward. At first, as shown in Figure 5, the maximum P_{out} and $Disp_{p-p}$ at a of 2.0 m/s^2 were as low as 0.021 μW and 28 μm, respectively, whereas the $Disp_{p-p}$ of the same harvester structure but without the FDE was 410 μm. As explained in the last part of the second section, the reason for the marked decrease in the $Disp_{p-p}$ value is that the extremely strong FDE electrostatic force attracts the oscillator onto the stoppers and suppresses its movement. Thus, as the level of the applied acceleration increases, the oscillator become more movable by overcoming the attracting force of the FDE, which increases the output power and widens the frequency band. The maximum output power and the half-power frequency bandwidth at a of 9.8 m/s^2 are 54 μW and 13 Hz, respectively.

We will compare the performance of the developed harvester with the state-of-the-art. For practical reasons, we chose references in which the resonance frequency is less than 200 Hz and the output power is greater than 0.1 μW. In general, the output power of vibration energy harvesters depends on the device configuration (the inertial mass m, and the volume V of the harvester) and the vibrational conditions [the applied displacement A (or the applied acceleration a), and the resonance frequency f_r]. To discuss the potential of the FDE-based harvester except for the device configuration and the vibrational conditions, this study employs the following normalization based

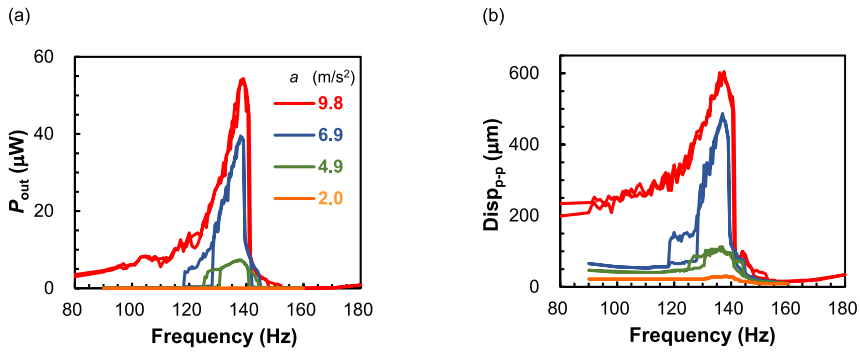

FIG. 5. (a) Output power P_{out} and (b) peak-to-peak displacement $Disp_{p-p}$ of the oscillator versus frequency with various acceleration values a.

TABLE I. Comparison of this work to the state-of-the-art. The unit of the figure of merit (*FOM*) is μW·rad.·gram^{-1}·(m/s^2)$^{-2}$·cm^{-3}. Δf is the half-power frequency bandwidth. For reference, the data for a piezoelectric vibration energy harvester in Ref. 26 is added.

	Vibrational Direction	a (m/s^2)	f_r (Hz)	m (gram)	V (cm^3)	V_s (V)	P_{out} (μW)	Δf (Hz)	*FOM*
Masaki *et al.*[17]	In-plane	1.47	30	3.5[a]	6.4	-700	~150	3	590
Tao *et al.*[18]	In-plane	2	121/125	0.0699	0.54	-320	0.12	1.4[d]	623
Minakawa *et al.*[19]	In-plane	4.9	28	0.5	0.305[c]	-396	1.5	12	72
Matsumoto *et al.*[20]	In-plane	13.7	40	0.44[b]	0.305	-800	6	14	60
Suzuki *et al.*[21]	In-plane	9.8	38	0.44	0.305[c]	N/A	4	22	74
Boisseau *et al.*[22]	Out-of-plane	1	50	5	3.64	1400	50	0.7[d]	863
Chiu *et al.*[23]	Out-of-plane	19.6	110	0.358	0.484	-400	20.7	11[d]	206
Wang *et al.*[24]	Out-of-plane	9.8	98	0.07	0.286	-400	0.15	20	48
Asanuma *et al.*[10]	Out-of-plane	4.9	102.5	0.077	0.88	-420	4.0	6.5	1,580
Tao *et al.*[25]	Out-of-plane	5	66	0.0198	0.12	800	0.34	6.5	2,350
This work	**Out-of-plane**	**9.8**	**139**	**0.088**	**0.8**	**-922**	**54**	**13**	**6,980**
Aktakka *et al.*[26]	-	14.7	154	0.465	0.146	-	205	14.1	13,500

[a]Mass is calculated from the resonant frequency and the spring constant as reported in Ref. 17.
[b]Mass is assumed to be the same as reported in Ref. 21.
[c]Device volume is assumed to be the same as reported in Ref. 20.
[d]Calculated from the mechanical quality factor.

on the velocity-damped resonant generator (VDRG) model:[15,16]

$$FOM \equiv \frac{P_{out}}{mA^2{\omega_r}^3V} = \frac{P_{out}\omega_r}{ma^2V}, \tag{4}$$

where FOM is the abbreviation for figure of merit of output power, and ω_r is $2\pi f_r$. Table I lists specifications and performance of the electret-based vibration energy harvesters developed so far. Δf is the half-power frequency bandwidth. The data for other state-of-the-art VEHs are available in Ref. 2. Our harvester design incorporating the FDE and the designed spring achieves the highest FOM. As listed in Table I, Ref. 21 showed the largest Δf of 22 Hz; however, it is defined by the frequency bandwidth at the half power level of the maximum 4 μW. Under the same definition, the frequency bandwidth of our harvester is up to 77 Hz. Thus, our proposed harvester that combines the FDE and the nonlinear spring restoring force can yield both the highest output power and wide frequency band among current electret-based vibration energy harvesters. Our harvester exhibited the highest FOM in electret-based vibration energy harvesters developed so far, however, its value is not still sufficient compared with those of other transduction technologies. For example, the FOM of the miniature piezoelectric vibration energy harvester calculated by the same VDRG

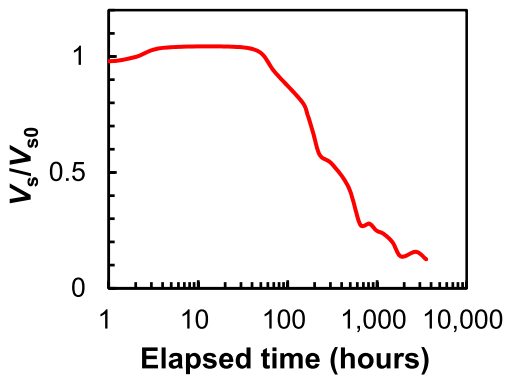

FIG. 6. Surface potential decay of the FDE normalized with initial value V_{s0}.

model is 13,500.[26] Our future work focuses on further increasing the FOM by optimizing the mass weight, spring constant, and poling process of the ferroelectric material. Through these future investigations, we hope to catch up with other transduction technologies.

Finally, we will discuss the stability of the FDE. As proved by our research, the FDE is very attractive material to achieve a high performance electrostatic vibration energy harvester. However, the stability of the FDE was not yet comparable to that of conventional polymer-based or inorganic silicon-based electrets. Figure 6 shows the surface potential decay of the FDE normalized with initial value V_{s0}. We used environment control system (Espec Co., Japan, SH-641) to keep temperature and relative humidity constant at 20 °C and 60 %RH, respectively. Recently, we revealed that the FDE formed from a hard PZT ceramic exhibited longer stability in surface potential than that of the FDE formed from a soft one, and the result may be attributed to the hardening of the domain wall motion due to the defect dipole pinning.[8] We can achieve greater stability by using a FDE prepared from harder ferroelectrics (with higher coercive electric field and Curie temperature) and by optimizing the poling process (applied voltage, temperature, and treatment time). This is our future work as well as the increase in FOM of our harvester.

IV. CONCLUSION

In this study, we propose and design a spring with a stopper to prevent the pull-in caused by the strong electrostatic force of the FDE, and evaluate performance of a vibration energy harvester that combines the FDE and the spring. The FEM analysis validated that the restoring force of the designed spring exceeds the estimated electrostatic force of the FDE, and thus the designed spring can prevent the pull-in for the FDE-based vibration energy harvester. A practical harvester combines the FDE and the spring successfully, and generated electricity without pull-in. The maximum output power and the half-power frequency bandwidth at an acceleration of 9.8 m/s^2 are 54 μW and 13 Hz, respectively. Furthermore, our harvester achieved both the highest FOM of output power and the wide frequency band, compared with other electret-based vibration energy harvesters developed to date.

ACKNOWLEDGEMENTS

We would like to thank the Japan Society for the Promotion of Science (JSPS). This work was supported by a Grant-in-Aid for JSPS fellows (No. 254346).

[1] R. Bogue, Sensor Review **34**, 137 (2014).
[2] S. Boisseau, G. Despesse, and B. A. Seddik, in *Electrostatic Conversion for Vibration Energy Harvesting, Small-Scale Energy Harvesting*, edited by Dr. Mickaël Lallart (InTech, Rijeka, 2012), p. 91.
[3] S.G. Kim, S. Priya, and I. Kanno, MRS BULLETIN **37**, 1039 (2012).
[4] S.P. Beeby, R.N. Torah, M.J. Tudor, P. Glynne-Jones, T. O'Donnell, C.R. Saha, and S. Roy, J. Micromech. Microeng. **17**, 1257 (2007).
[5] T. Ueno, J. Appl. Phys. **117**, 17A740 (2015).
[6] H. Asanuma, H. Oguchi, M. Hara, R. Yoshida, and H. Kuwano, Appl. Phys. Lett. **103**, 162901 (2013).
[7] H. Asanuma, H. Oguchi, M. Hara, and H. Kuwano, in *Proceedings of The 17th International Conference on Solid-State Sensors, Actuators and Microsystems (TRANSDUCERS), Barcelona, Spain, 16-20 Jun 2013*, pp. 1332–5.
[8] H. Asanuma, H. Oguchi, M. Hara, and H. Kuwano, in *Proceedings of The 13th International Conference on Micro and Nanotechnology for Power Generation and Energy Conversion Applications (PowerMEMS 2013), London, UK, 3-6 Dec 2013*, pp. 192–6.
[9] C. Son and B. Ziaie, Appl. Phys. Lett. **92**, 013509 (2008).
[10] H. Asanuma, M. Hara, H. Oguchi, and H. Kuwano, J. Micromech. Microeng. **25**, 104013 (2015).
[11] T. Seki, Y. Uno, K. Narise, T. Masuda, K. Inoue, S. Sato, F. Sato, K. Imanaka, and S. Sugiyama, Sensors and Actuators A **132**, 683 (2006).
[12] M. S. M. Soliman, E. M. Abdel-Rahman, E. F. El-Saadany, and R. R. Mansour, Journal of Microelectromechanical Systems **18**, 1288 (2009).
[13] Z. Zeng, B. Ren, Q. Xu, D. Lin, W. Di, H. Luo, and D. Wang, Appl. Phys. Lett. **107**, 173502 (2015).
[14] H. Asanuma, M. Hara, H. Oguchi, and H. Kuwano, in *Proceedings of the 14th International Conference on Micro and Nanotechnology for Power Generation and Energy Conversion Applications (PowerMEMS 2014), Awaji Island, Hyogo, Japan, 18-21 Nov 2014*, pp. 595–9.
[15] C.B. Williams and R.B. Yates, Sensors and Actuators A **52**, 8 (1996).
[16] P.D. Mitcheson, E.M. Yeatman, G.K. Rao, A.S. Holmes, and T.C. Green, Proceedings of the IEEE **96**, 1457 (2008).

[17] T. Masaki, N. Yoshitake, S. Kamiyama, M. Nabeto, T. Seki, M. Oba, and D. Uchida, in *Proceedings of the 14th International Conference on Micro and Nanotechnology for Power Generation and Energy Conversion Applications (PowerMEMS 2014)*, *Awaji Island, Hyogo, Japan*, *18-21 Nov 2014*, pp. 352–6.
[18] K. Tao, J. Miao, S. W. Lye, and X. Hu, Sensors and Actuators A **228**, 95 (2015).
[19] Y. Minakawa, R. Chen, and Y. Suzuki, in *Proceedings of The 17th International Conference on Solid-State Sensors, Actuators and Microsystems (TRANSDUCERS & EUROSENSORS 2013)*, *Spain, Barcelona*, *16-20 June 2013*, pp. 2241–4.
[20] K. Matsumoto, K. Saruwatari, and Y. Suzuki, in *Proceedings of the 14th International Conference on Micro and Nanotechnology for Power Generation and Energy Conversion Applications (PowerMEMS 2011)*, *Seoul, Republic of Korea*, *15-18 Nov 2011*, pp. 134–7.
[21] Y. Suzuki and S. Kawasaki, in *Proceedings of the 5th European Conference on Antennas and Propagation (EUCAP)*, *Rome, Italy*, *11-15 Apr 2011*, pp. 3897–3900.
[22] S. Boisseau, G. Despesse, T. Ricart, E. Defay, and A. Sylvestre, Smart Mater. Struct. **20**, 105013 (2011).
[23] Y. Chiu and Y. C. Lee, J. Micromech. Microeng. **23**, 015012 (2013).
[24] F. Wang and Ole Hansen, Sensors and Actuators A **211**, 131 (2014).
[25] K. Tao, S. W. Lye, J. Miao, and X. Hu, Microelectronic Engineering **135**, 32 (2015).
[26] E.E. Aktakka, R.L. Peterson, and K. Najafi, in *Proceedings of 16th International Solid-State Sensors, Actuators and Microsystems Conference (TRANSDUCERS)*, *Beijing, China*, *5-9 June 2011*, pp. 1649–52.